SANDIA REPORT
SAND2011-4247
Unlimited Release
Printed June 2011

Creating Dynamic Equivalent PV Circuit Models with Impedance Spectroscopy for Arc-Fault Modeling

Jay Johnson, David Schoenwald, Scott Kuszmaul, and Jason Strauch

Prepared by
Sandia National Laboratories
Albuquerque, New Mexico 87185 and Livermore, California 94550

Sandia National Laboratories is a multi-program laboratory managed and operated by Sandia Corporation, a wholly owned subsidiary of Lockheed Martin Corporation, for the U.S. Department of Energy's National Nuclear Security Administration under contract DE-AC04-94AL85000.

Approved for public release; further dissemination unlimited.

Sandia National Laboratories

Issued by Sandia National Laboratories, operated for the United ***S***tates Department of Energy by Sandia Corporation.

NOTICE: This report was prepared as an account of work sponsored by an agency of the United States Government. Neither the United States Government, nor any agency thereof, nor any of their employees, nor any of their contractors, subcontractors, or their employees, make any warranty, express or implied, or assume any legal liability or responsibility for the accuracy, completeness, or usefulness of any information, apparatus, product, or process disclosed, or represent that its use would not infringe privately owned rights. Reference herein to any specific commercial product, process, or service by trade name, trademark, manufacturer, or otherwise, does not necessarily constitute or imply its endorsement, recommendation, or favoring by the United States Government, any agency thereof, or any of their contractors or subcontractors. The views and opinions expressed herein do not necessarily state or reflect those of the United States Government, any agency thereof, or any of their contractors.

Printed in the United States of America. This report has been reproduced directly from the best available copy.

Available to DOE and DOE contractors from
U.S. Department of Energy
Office of Scientific and Technical Information
P.O. Box 62
Oak Ridge, TN 37831

Telephone: (865) 576-8401
Facsimile: (865) 576-5728
E-Mail: reports@adonis.osti.gov
Online ordering: http://www.osti.gov/bridge

Available to the public from
U.S. Department of Commerce
National Technical Information Service
5285 Port Royal Rd.
Springfield, VA 22161

Telephone: (800) 553-6847
Facsimile: (703) 605-6900
E-Mail: orders@ntis.fedworld.gov
Online order: http://www.ntis.gov/help/ordermethods.asp?loc=7-4-0#online

SAND2011-4247
Unlimited Release
Printed June 2011

Creating Dynamic Equivalent PV Circuit Models with Impedance Spectroscopy for Arc-Fault Modeling

Jay Johnson, David Schoenwald, Scott Kuszmaul, and Jason Strauch

Sandia National Laboratories
P.O. Box 5800
Albuquerque, New Mexico 87185-MS1321

Abstract

Article 690.11 in the 2011 *National Electrical Code®* *(NEC®)* requires new photovoltaic (PV) systems on or penetrating a building to include a listed arc fault protection device. Currently there is little experimental or empirical research into the behavior of the arcing frequencies through PV components despite the potential for modules and other PV components to filter or attenuate arcing signatures that could render the arc detector ineffective. To model AC arcing signal propagation along PV strings, the well-studied DC diode models were found to inadequately capture the behavior of high frequency arcing signals. Instead dynamic equivalent circuit models of PV modules were required to describe the impedance for alternating currents in modules. The nonlinearities present in PV cells resulting from irradiance, temperature, frequency, and bias voltage variations make modeling these systems challenging. Linearized dynamic equivalent circuits were created for multiple PV module manufacturers and module technologies. The equivalent resistances and capacitances for the modules were determined using impedance spectroscopy with no bias voltage and no irradiance. The equivalent circuit model was employed to evaluate modules having irradiance conditions that could not be measured directly with the instrumentation. Although there was a wide range of circuit component values, the complex impedance model does not predict filtering of arc fault frequencies in PV strings for any irradiance level. Experimental results with no irradiance agree with the model and show nearly no attenuation for 1 Hz to 100 kHz input frequencies.

ACKNOWLEDGMENTS

This work was funded by the US Department of Energy Solar Energy Technologies Program.

CONTENTS

1. INTRODUCTION 7
2. DYNAMIC PV MODULE MODELING 8
3. DYNAMIC MODEL GENERATION 10
4. MODELING ARC FAULT FREQUENCY RESPONSE 16
5. CONCLUSIONS 20
6. REFERENCES 21
DISTRIBUTION 23

FIGURES

Figure 1. Propagation of arcing signal through a PV string. 7
Figure 2. Equivalent dynamic electrical circuit for a PV module[11]. 8
Figure 3. Simplified dynamic electric circuit for a PV module. $C_D \parallel C_T = C_p$ and $R_d \parallel R_{sh} = R_p$. ... 8
Figure 4. Complex impedance for Module H with the equivalent circuit model. 11
Figure 5. Complex impedance for Module D with frequencies labeled in Hz. For increasing frequency, the impedance spectroscopy plot is traced from the right to the left. (Note the 120 Hz noise from the instrument is visible in the trace.) 11
Figure 6. Reactance vs frequency for Module D and reactance models with C_p = 0.2, 0.5, and 1 μF. C_p = 0.5 μF minimized the error between the model and the experimental data. 12
Figure 7. Complex impedance of multiple modules. 13
Figure 8. Amorphous Si module impedance compared to crystalline Si modules. 13
Figure 9. Complex impedance of a large number of p-Si modules with a 250 mV input. 14
Figure 10. Complex impedance of multiple p-Si modules with a 1.50 V input. 15
Figure 11. Frequency response configuration with an equivalent PV model with no irradiance. 16
Figure 12. Dynamic PV model in Simulink. 16
Figure 13. Bode plot of Module D from 1 Hz to 100 kHz using the equivalent dynamic circuit values from impedance spectroscopy. None of the simulated modules show filtering. 17
Figure 14. Dynamic PV model of 72 PV cells in series (3 sets of 24 cells) in Simulink. 18
Figure 15. Bode plot of 72 PV cells in series from 1 Hz to 100 GHz. The simulated array panel shows no filtering effects until very high frequencies. 18
Figure 16. Experimental frequency responses for the eight modules. 19

TABLES

Table 1. Modules and equivalent circuit values 10

NOMENCLATURE

AC	Alternating Current
DC	Direct Current
DOE	Department of Energy
NEC	National Electric Code
PV	Photovoltaic
SNL	Sandia National Laboratories

1. INTRODUCTION

Sandia National Laboratories is researching the electromagnetic propagation characteristics of arcing signals through PV arrays in order to (a) inform arc fault detector designers of frequency-dependent PV attenuation, electromagnetic noise, and radio frequency (RF) effects within PV systems, and (b) to determine if there are preferred frequency bandwidths for arc fault detection. In order to provide this information, the AC frequency response of PV modules, strings, and conductors is being characterized. This paper specifically focuses on the filtering effects of PV modules.

Modeling the frequency response of PV modules must account for unique PV cell responses at different irradiances, temperatures, currents, and voltages. Modeling the dynamic (AC) equivalent circuit of modules helps to better understand when there is frequency-dependent attenuation through PV strings. As illustrated in Figure 1, an arc generates a range of AC arcing noise on top of the PV DC current. This signal travels down the PV string through the modules to the arc fault circuit interrupter (AFCI). As the signal passes through the modules, the arc signature may be attenuated, which could result in inaccurate arc fault detection when a modified AC arcing signal reaches a remotely-located detector.

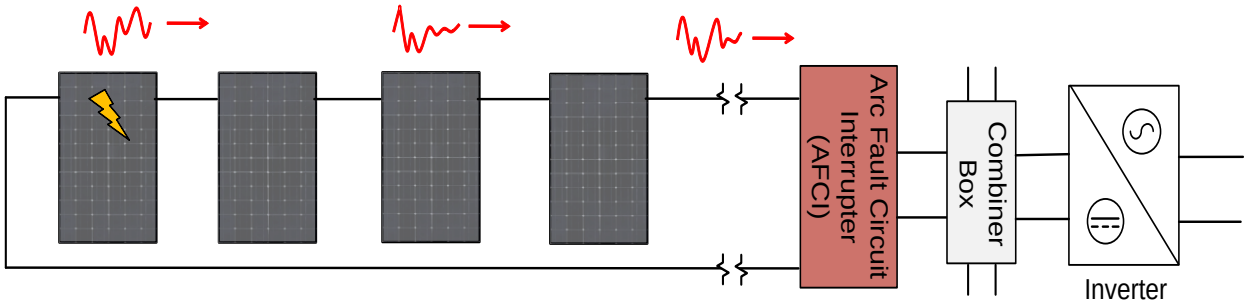

Figure 1. Propagation of arcing signal through a PV string.

2. DYNAMIC PV MODULE MODELING

AC models of PV systems have been previously studied to characterize their use as optical detectors [1], measure cell layers [2-3], determine charge densities [4], and to observe how the resistances and capacitances change with varying cell inputs such as illumination [5] and temperature [6-7]. The dynamic circuits have been developed based on different semiconductor models (e.g., carrier physics [1]), but to determine the values for the circuit components, time-domain [7-10] or frequency domain techniques [9, 11-12] are used. One dynamic equivalent circuit model and the simplified electrical circuit model are shown in Figure 2 [10-13], where:

I_{mod}	=	module current
R_s	=	series resistance
R_{sh}	=	shunt resistance
$R_d(V)$	=	dynamic resistance of diode
$C_D(V,\omega)$	=	diffusion capacitance
$C_T(V)$	=	transition capacitance
V_{ac}	=	dynamic voltage
ω	=	signal frequency

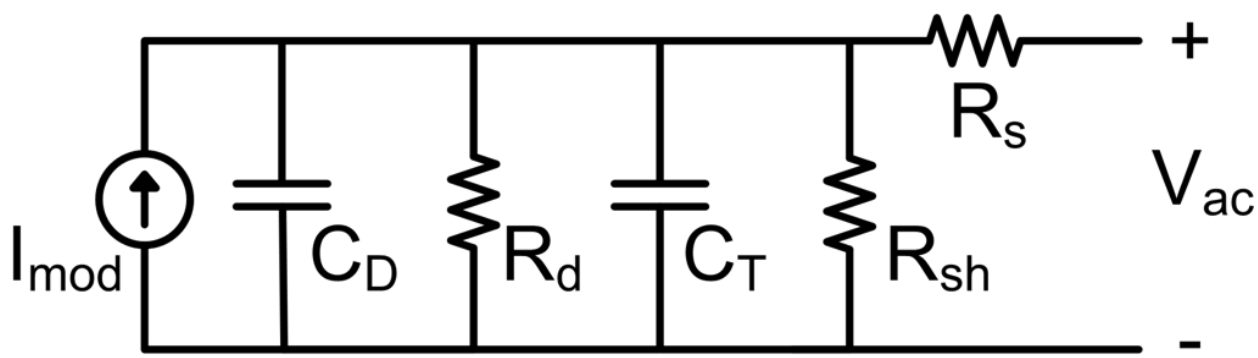

Figure 2. Equivalent dynamic electrical circuit for a PV module[11].

This model can be simplified by combining electrical components, as shown in Figure 3.

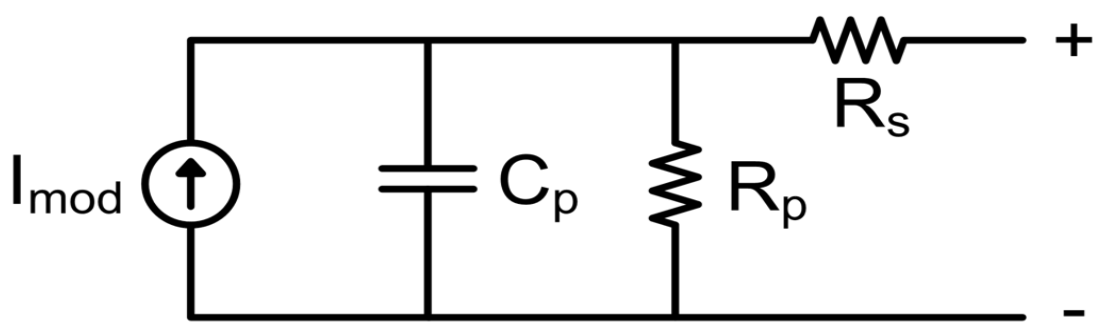

Figure 3. Simplified dynamic electric circuit for a PV module. C_D || C_T=C_p and R_d || R_{sh}= R_p.

Chenvidhya et al. [14] calculated the equivalent complex impedance to be

$$Z_{PV} = \left[R_s + \frac{R_P}{\left(\omega R_P C_P\right)^2 + 1} \right] - j \left[\frac{\omega R_P^2 C_P}{\left(\omega R_P C_P\right)^2 + 1} \right] \quad (1)$$

However, some of these electrical components are not static values with respect to frequency and bias voltage. Chenvidhya *et al.* determined the circuit components were significantly affected by bias voltage [15] and Chayavanich *et al.* determined there was voltage and frequency dependence on the transition and diffusion capacitance [7]. Thus, resistance and reactance of Eq. (1) are functions of voltage and frequency.

In order to determine the resistance and capacitance values, many researchers use impedance spectroscopy [9, 12]. The resistor values are determined by studying the dynamic impedance loci: R_s is the high frequency intercept and $R_s + R_p$ intercept is at the minimum frequency [16]. The combined capacitance, C_p, can be calculated from the measured reactance.

3. DYNAMIC MODEL GENERATION

Four polycrystalline-silicon (p-Si), one amorphous-silicon (a-Si), and three crystalline-silicon (c-Si) modules were scanned with the frequency response analyzer from 1 Hz to 100 kHz to produce equivalent AC models. The input sinusoid was 250 mV. Testing was conducted at room temperature, and there were no irradiance or bias voltage influences on the module. A list of the tested modules and the measured resistance and capacitance values appear in Table 1.

Table 1. Modules and equivalent circuit values

Module	Cell Type	P_{max} (W)	R_p (kΩ)	R_s (Ω)	C_p (μF)	Minimum Reactance Frequency
Module A	p-Si	72.0	4.27	0.50	1.8	355 kHz
Module B	p-Si	47.8	2.10	0.83	1.6	328 kHz
Module C	p-Si	72.3	1.08	1.02	4.0	194 kHz
Module D	c-Si	175	13.2	6.81	0.5	118 kHz
Module E	c-Si	75.0	3.65	0.31	1.8	188 kHz
Module F	c-Si	200	5.60	1.29	2.4	576 kHz
Module G	a-Si	43.0	348	13.8	3.4	666 kHz
Module H	p-Si	93.6	17.3	2.21	2.2	531 kHz

In order to determine the circuit element parameters, the complex impedance of the modules was recorded with an AP Instruments Model 300 Frequency Response Analyzer. The complex impedance plot for Module H is shown in Figure 4. The intercepts along the resistance axis correspond to R_s when the frequency approaches infinity ($\omega \rightarrow \infty$) and $R_s + R_p$ when the frequency is 0 ($\omega = 0$), as shown in Figure 5.

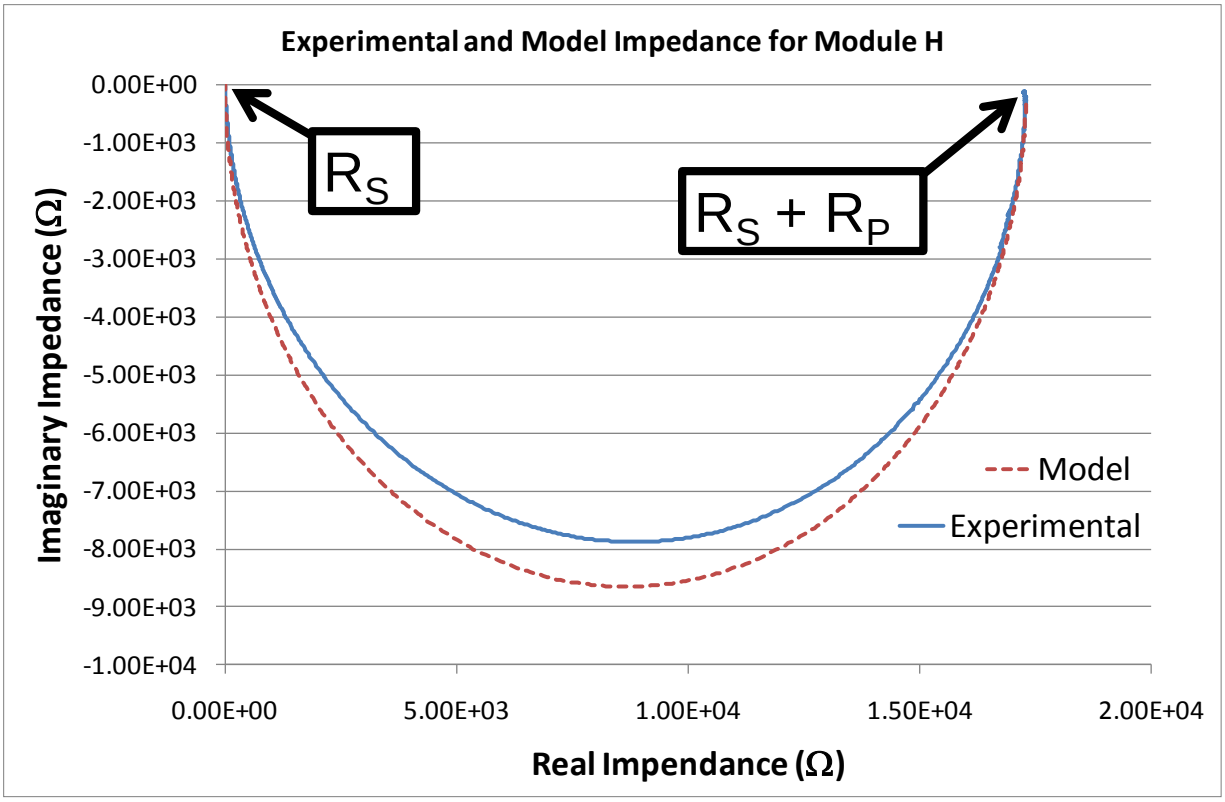

Figure 4. Complex impedance for Module H with the equivalent circuit model.

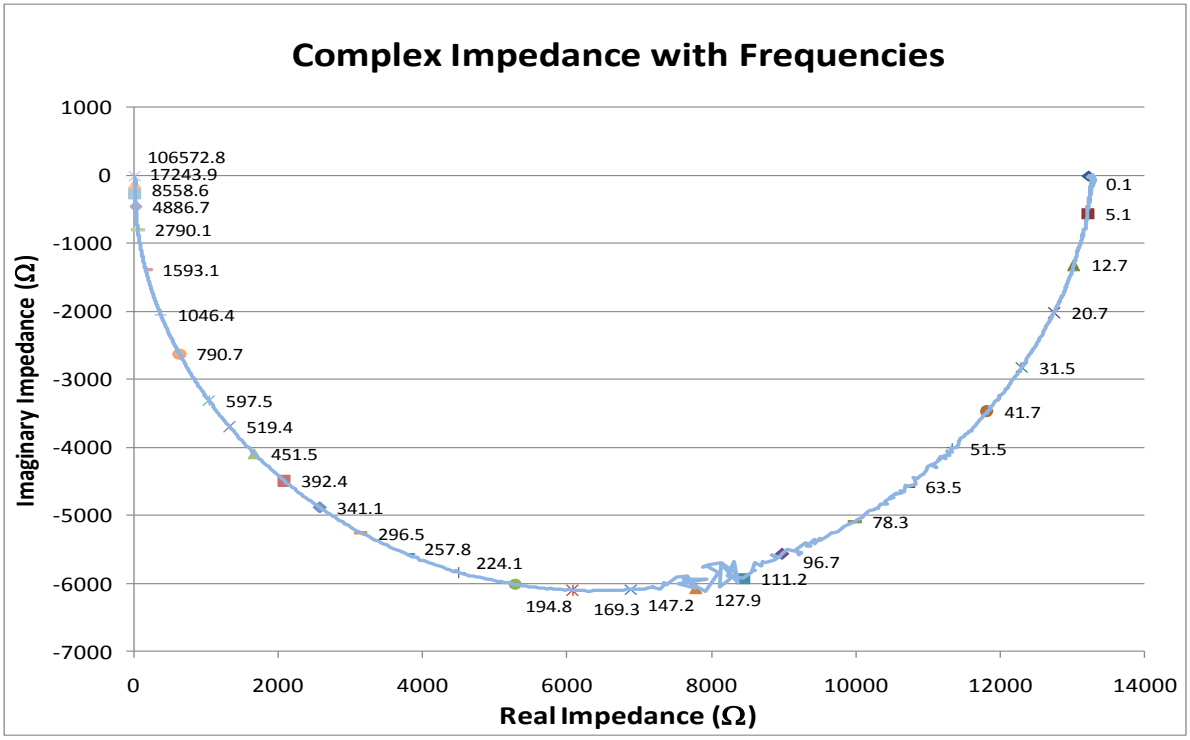

Figure 5. Complex impedance for Module D with frequencies labeled in Hz. For increasing frequency, the impedance spectroscopy plot is traced from the right to the left. (Note the 120 Hz noise from the instrument is visible in the trace.)

To determine the value of C_p, the error between the model and the experimental results were minimized, shown in Figure 6. The minimization can be performed in a number of different ways but the technique used here was a minimizing routine based on the difference between the reactance of the model and the data for all frequencies for which data were collected, given by

$$Z_{PV} = \min\left\{ \sum_{f=f_1}^{f_{final}} \left| \mathrm{Im}\left[Z_{PV}^{Model}(f)\right] - \mathrm{Im}\left[Z_{PV}^{Data}(f)\right] \right| \right\} \quad (2)$$

where f is the frequency in Hz, f_1 is the first experimentally measured frequency, f_{final} is the last measured frequency, $\mathrm{Im}\left[Z_{PV}^{Model}(f)\right]$ is the reactance of the model at frequency f, and $\mathrm{Im}\left[Z_{PV}^{Data}(f)\right]$ is the reactance of the data at frequency f.

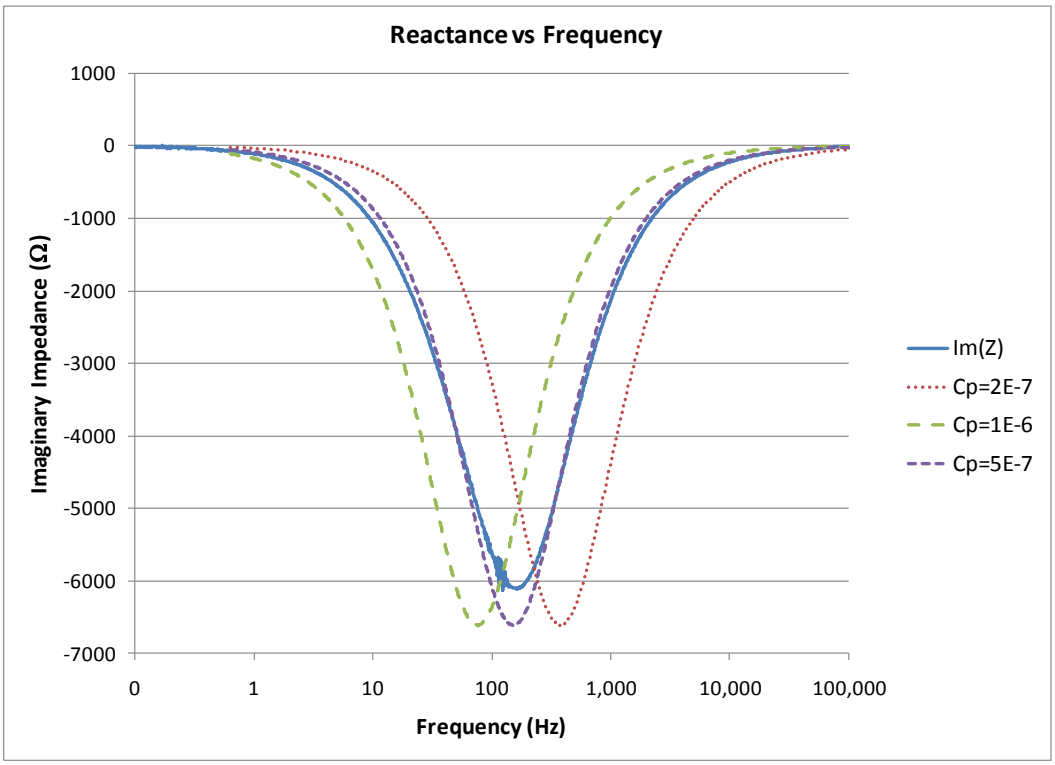

Figure 6. Reactance vs frequency for Module D and reactance models with C_p = 0.2, 0.5, and 1 μF. C_p = 0.5 μF minimized the error between the model and the experimental data.

The large variability in module impedances for different PV technologies and manufacturers is seen in the comparison in Figure 7. This is expected as C_D, C_T, and R_d are known to vary with temperature, light, voltage and cell materials [9]. The R_p resistance varies significantly between each of the modules, shown by the difference in the low frequency intercepts. The amorphous silicon module had much larger R_s and R_p values in comparison to the other modules, shown in Figure 8. The series resistance for each of the modules is more than three orders of magnitude smaller than the combined dynamic and shunt resistances. There was also significant variability between the modules for the parallel capacitance (C_p) values.

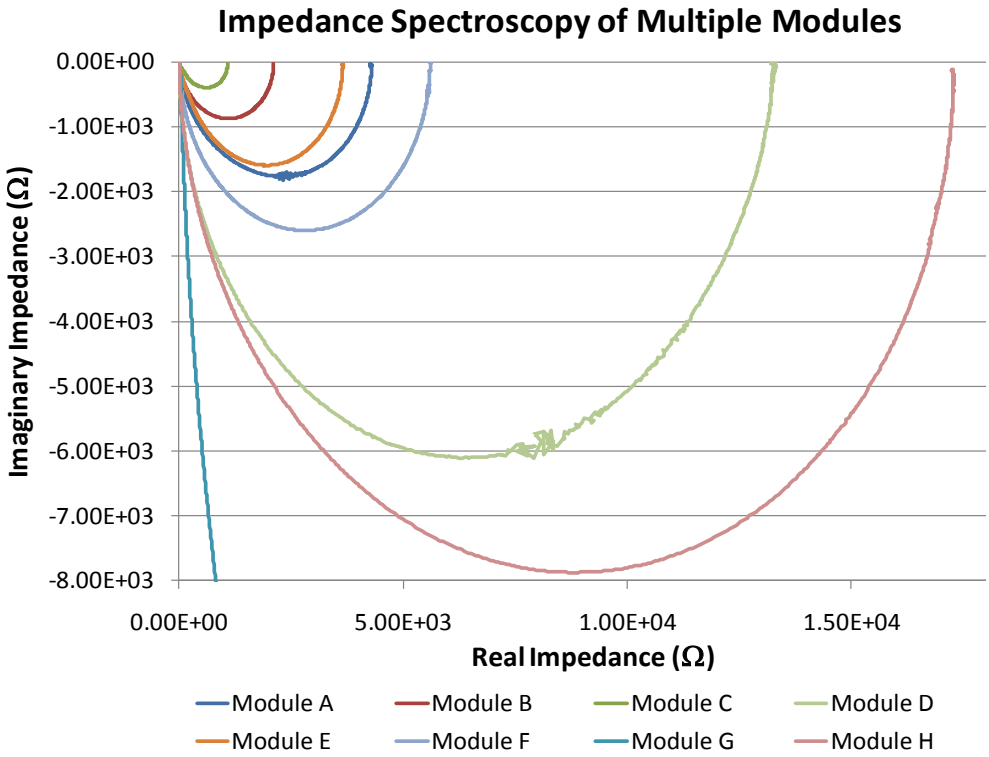

Figure 7. Complex impedance of multiple modules.

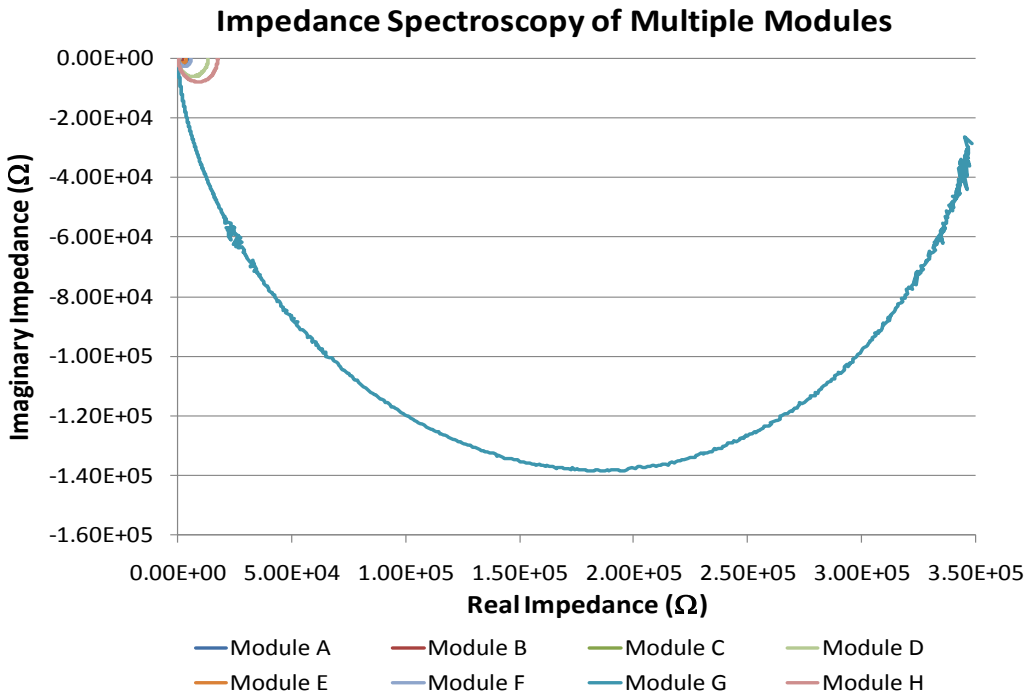

Figure 8. Amorphous Si module impedance compared to crystalline Si modules.

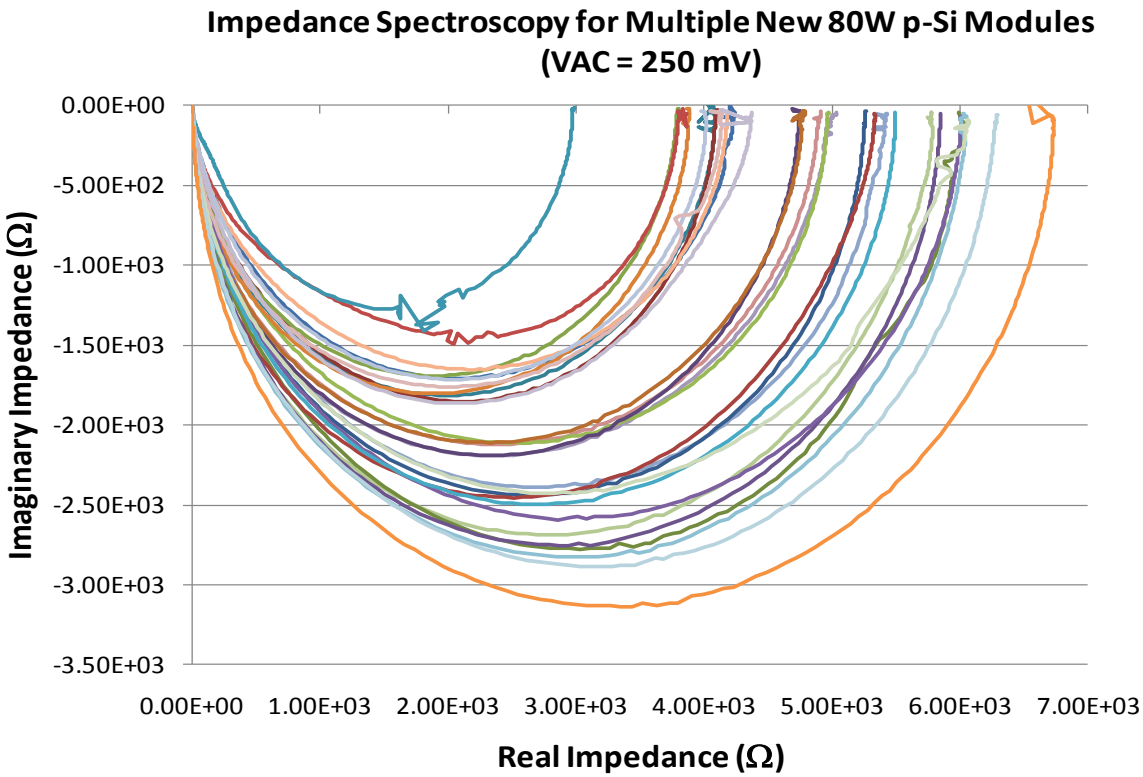

Figure 9. Complex impedance of a large number of p-Si modules with a 250 mV input.

In order to quantify the variability in module impedances for the same PV production process 28 80-W p-Si modules were analyzed. Repeatability was good. The large range of impedance spectroscopy results shown in Figure 9 was due to cell binning [17], bypass diode variability, and manufacturing variability.

To calculate the voltage dependency of the module impedance, the same set of p-Si modules was used with a 1.50 V impedance spectroscopy input signal. Comparing the 250 mV results to the 1.50 V results in Figure 10, the impedance magnitude is seen to be significantly smaller with higher voltage signals. The average R_p value decreased from 4.89 kΩ to 3.31 kΩ indicating the higher voltage had less resistance through the cells. Since the AC input voltage influenced the results significantly, it is believed that the module impedance will also drastically change with irradiance because it will adjust the module bias voltage along the I-V curve.

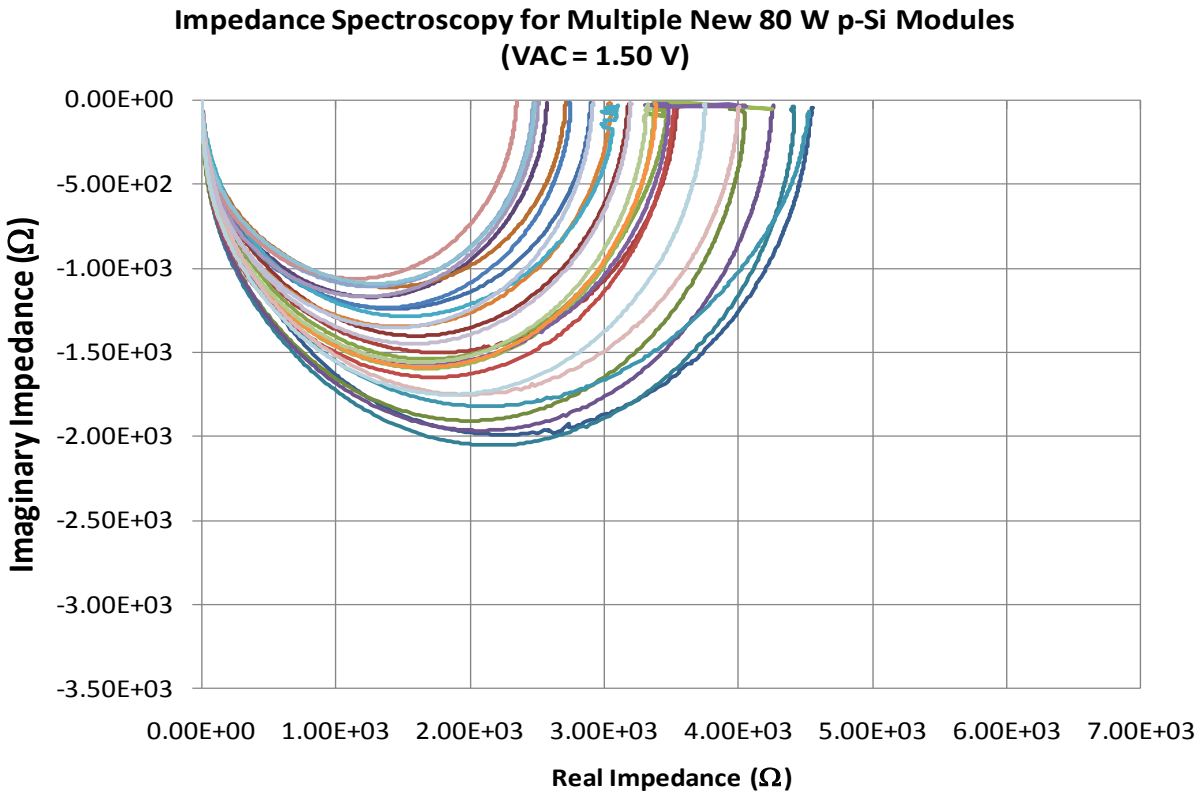

Figure 10. Complex impedance of multiple p-Si modules with a 1.50 V input.

4. MODELING ARC FAULT FREQUENCY RESPONSE

Simulations of the equivalent dynamic models were performed with MATLAB®/Simulink® to identify the attenuation effects of the PV modules. The different module circuits were analyzed for filtering effects using the circuit parameters determined from the impedance spectroscopy measurements in Table 1. In order to generate the attenuation data for the modules, the circuit shown in Figure 11, was built using Simscape™ components in Simulink, as shown in Figure 12. Since impedance spectroscopy and frequency response analysis of the modules were performed with no irradiance on the module, the *DC Current Source* was removed from the model for tests without irradiance. The simulation was run with and without bypass diodes, and probe resistance and capacitance. The model was then linearized with Simulink Control Design using the input sinusoid and output voltage as control points. Bode plots were generated for frequencies from 1 Hz to 100 kHz for each of the modules. The Bode plots for all simulated modules show no attenuation or filtering. The Bode plot for Module D is shown in Figure 13. The results show no filtering for all simulated modules.

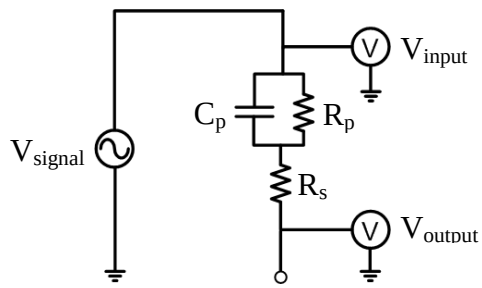

Figure 11. Frequency response configuration with an equivalent PV model with no irradiance.

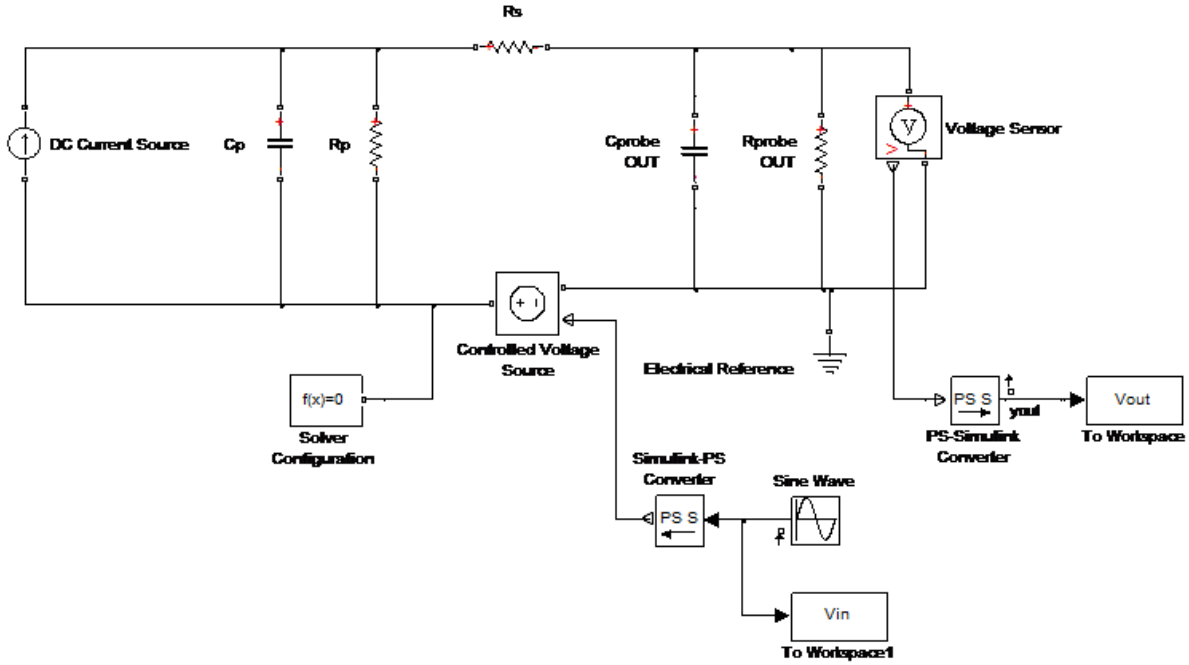

Figure 12. Dynamic PV model in Simulink.

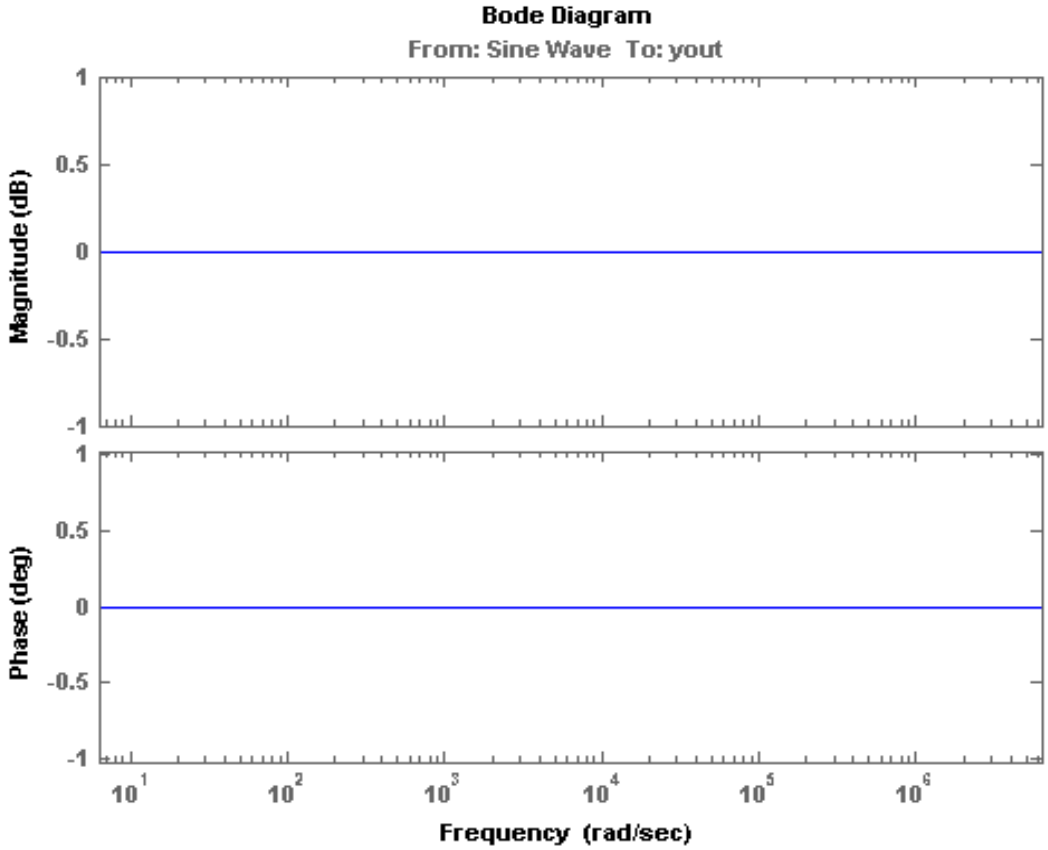

Figure 13. Bode plot of Module D from 1 Hz to 100 kHz using the equivalent dynamic circuit values from impedance spectroscopy. None of the simulated modules show filtering.

For further study, simulations of three sets of 24 PV cells in series (each set with a bypass diode) were modeled with equivalent single cell circuit parameters to those of Module D. The purpose of these simulations was to determine if the explicit modeling of interconnections between the PV cells would change the frequency response of the modules. Figure 14 shows the Simscape™ components in Simulink needed to produce the model. Each PV array series string contains 24 circuits connected as in Figure 3. The simulations were performed with no irradiance on any of the PV cells with the exact same values for the probe resistance and capacitance. Figure 15 illustrates the Bode plots which show no filtering until very large signal frequencies (10s of GHz range) at which point the nonzero probe capacitance (25 pF in this case) and finite probe resistance (100kΩ in this case) begin to show a 20 dB/decade rolloff. This frequency range is generally well beyond the frequency range of interest.

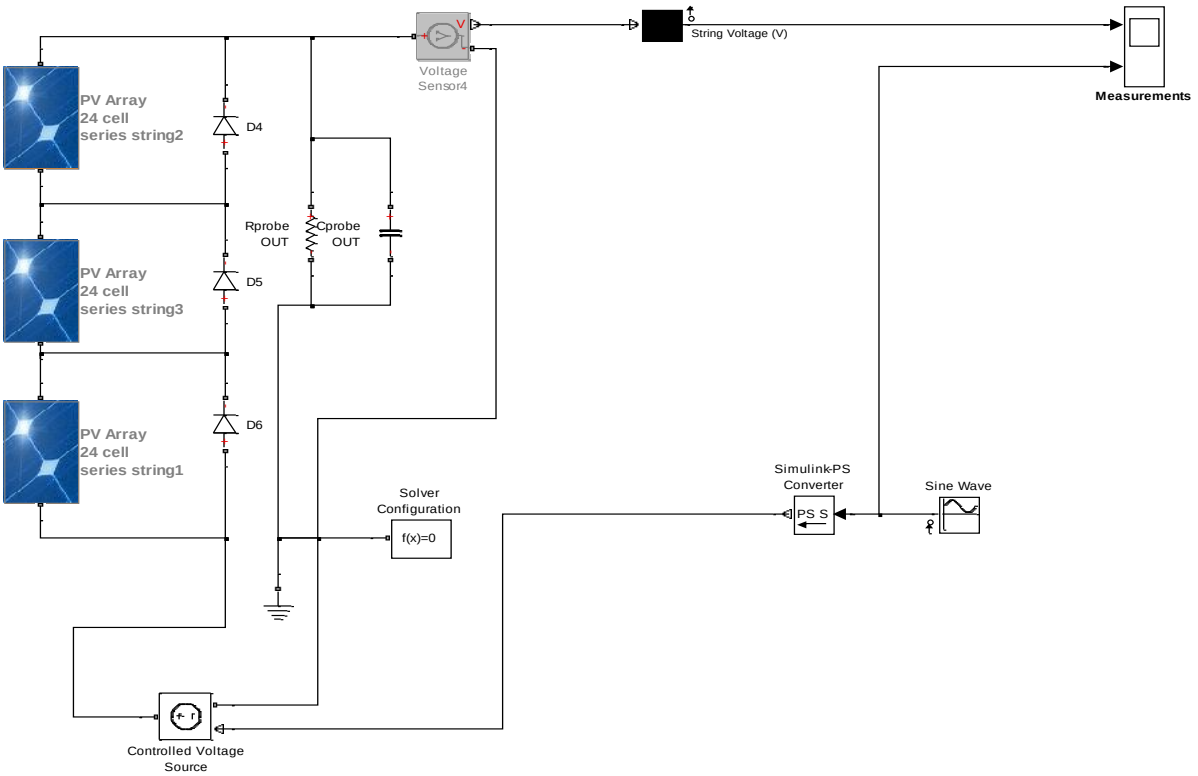

Figure 14. Dynamic PV model of 72 PV cells in series (3 sets of 24 cells) in Simulink.

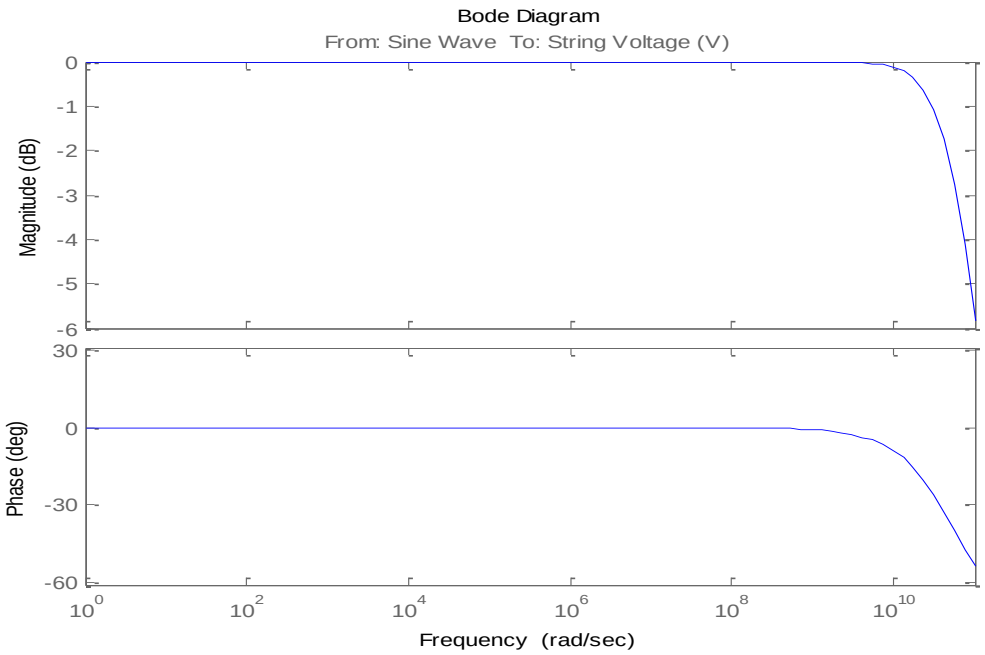

Figure 15. Bode plot of 72 PV cells in series from 1 Hz to 100 GHz. The simulated array panel shows no filtering effects until very high frequencies.

The results from the MATLAB/Simulink simulations were compared to frequency response data collected for the modules using the AP Instruments Frequency Response Analyzer. The experimental data, shown in Figure 16, was collected under the same conditions as the impedance spectroscopy data—at room temperature with no irradiance. There was agreement between the simulations and the frequency response data. The equivalent circuitry does not filter the passing arc fault frequencies for all the crystalline and polycrystalline modules. However, there is a small amount of high-pass filtering for the amorphous-Si module. The cause of this filtering effect is unknown, but it may be a result of bypass diodes or other nonlinearities that were not captured in the dynamic PV model.

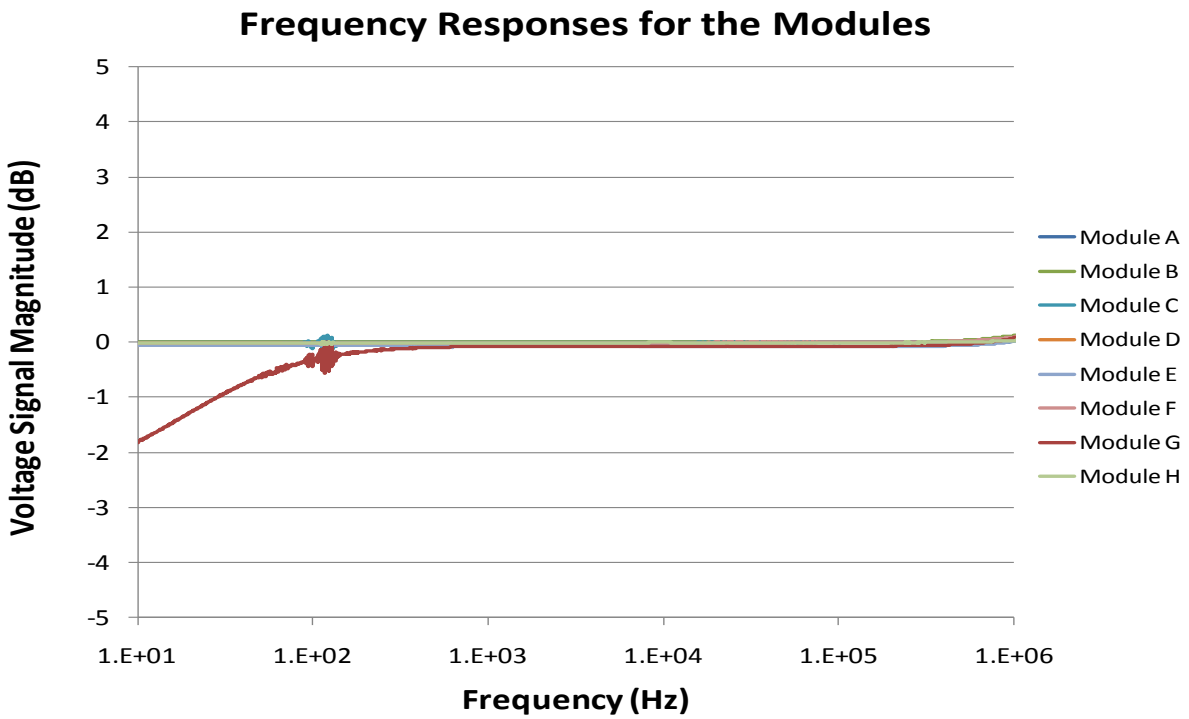

Figure 16. Experimental frequency responses for the eight modules.

Due to limitations of the instrumentation, frequency response characterization of the modules with irradiance was not possible without using DC blocking hardware. This hardware unfortunately interferes with the data collection as it introduces additional electrical components through which the signal must be transmitted. However, using the Simulink model, it was possible to simulate varying degrees of irradiance by increasing the value of the *DC Current Source*. For all irradiance values, there was no attenuation for frequencies between 1 Hz and 100 kHz.

5. CONCLUSIONS

Equivalent AC circuits were created for modeling the frequency response of PV modules. This study employed a theoretical framework using impedance spectroscopy to determine the equivalent circuit models that were then used to model the dynamic effects present in PV arrays. The numerical simulation results matched experimental frequency response data for the zero irradiance case. The simulations were then expanded to situations with higher irradiances for which impedances could not be directly measured. The circuit models determined that arcing frequencies in PV systems would not be attenuated prior to reaching a remotely located arc fault detector. In all simulations there was no appreciable filtering or attenuations through the PV module models.

The following recommendations and observations are made:

1. Impedance spectroscopy is helpful in matching module behavior to the equivalent circuit models.
2. A small database of equivalent circuits is now available for modeling the frequency response of modules.
3. Dynamic PV models can be used in MATLAB/Simulink, SPICE, or other analog circuit modeling software package.
4. Simulated circuits can be used to determine if arcing frequencies in PV systems are being filtered by the PV components prior to reaching a remotely located arc fault detector.
5. There is significant impedance variability between PV module manufacturers, technologies, and modules in the same module family.
6. Voltage and frequency dependencies are difficult to model. (A transmission line model may be used to account for these dependencies.)

Further study is needed in evaluating other influences of the propagation of arcing frequencies through PV systems. There are many other components in PV systems that could attenuate the arc fault signal. Furthermore, at higher frequencies there are antenna effects, crosstalk, and other RF effects that become a factor in the signal quality.

6. REFERENCES

1. L.A. Mallette and R.L. Phillips, "Modeling solar cells for use as optical detectors: background illumination effects," Appl. Opt. 17, 1786-1788 (1978).
2. L. Raniero, E. Fortunato, I. Ferreira, and R. Martins, "Study of nanostructured/amorphous silicon solar cell by impedance spectroscopy technique", Journal of Non-Crystalline Solids, Volume 352, Issues 9-20, Amorphous and Nanocrystalline Semiconductors - Science and Technology, 15 June 2006, Pages 1880-1883.
3. X. Zhang, J. Hu, Y. Wu and F. Lu, "Impedance spectroscopy characterization of proton-irradiated GaInP/GaAs/Ge triple-junction solar cells", 2010, *Semicond. Sci. Technol.* 25 035007.
4. Scofield, J.H., Contreras, M., Gabor, A.M., Noufi, R., and Sites, J.R., "Admittance measurements on Cu(In,Ga)Se_2 polycrystalline thin-film solar cells", *Photovoltaic Energy Conversion, 1994.*, vol.1, no., pp.291-294 vol.1, 5-9 Dec 1994.
5. R.A. Kumar, M. S. Suresh, and J. Nagaraju, "GaAs/Ge solar cell AC parameters under illumination", Solar Energy, Volume 76, Issue 4, April 2004, Pages 417-421.
6. V. Schlosser, and A. Ghitas. "Measurement of silicon solar cells ac parameters", Proceedings of the Arab Regional Solar Energy Conference (Manama, Bahrain, Nov 2006).
7. T. Chayavanich, C. Limsakul, N. Chayavanich, D. Chenvidhya, C. Jivacate, and K. Kirtikara, "Voltage and frequency dependent model for PV module dynamic impedance", 17th International Photovoltaic Science & Engineering Conference, 2007.
8. J. Thongpron, and K. Kirtikara, "Voltage and frequency dependent impedances of monocrystalline, polycrystalline and amorphous silicon solar cells," *Photovoltaic Energy Conversion, Conference Record of the 2006*, vol.2, no., pp. 2116-2119, May 2006.
9. D. Chenvidhya, K. Kirtikara, and C. Jivacate, "Dynamic impedance characterization of solar cells and PV modules based on frequency and time domain analysis", in Trends in solar energy research, Eds. Tom P. Hough, Nova Science Publishers, pp. 21-45, 2006.
10. M. P. Deshmukh, R. Anil Kumar, and J. Nagaraju, "Measurement of solar cell ac parameters using the time domain technique", Rev. Sci. Instrum. 75, 2732 (2004).
11. C. Limsakul, D. Chenvidhya, and K. Kirtikara, "PV impedance characterization using square wave method and frequency response analyser", *PVSEC15*, 10-16 October 2005, Shanghai, China.
12. R. Anil Kumar, M. S. Suresh, and J. Nagaraju, "Facility to measure solar cell ac parameters using an impedance spectroscopy technique", Rev. Sci. Instrum. 72, 3422 (2001).
13. H.S. Rauschenbach, Solar Cell Array Design Handbook, Van Nostrand Reinhold, New York, 1980.
14. D. Chenvidhya, C. Limsakul, J. Thongpron, K. Kirtikara, and C. Jivacate, 'Determination of solar cell dynamic parameters from time domain responses", 14th International Photovoltaic Science and engineering Conference, Jan 2004.
15. D. Chenvidhya *et al.*, 'PV module dynamic impedance and its voltage and frequency dependencies", *Solar Energy Materials & Solar Cells* **86** (2005), pp. 243–251.
16. C. Limsakul, N. Chayavanich, D. Chenvidhya, and K. Kirtikara, "PV impedance characterization using square wave method and frequency response analyzer", 15th International Photovoltaic Science & Engineering Conference, Oct 05.

17. H. Field, and A.M. Gabor, "Cell binning method analysis to minimize mismatch losses and performance variation in Si-based modules," Twenty-Ninth IEEE Photovoltaic Specialists Conference, 2002. pp. 418- 421, 19-24 May 2002.

DISTRIBUTION

1	MS0321	Robert W. Leland	01400
1	MS0321	John L. Mitchiner	01460
1	MS0352	Jay Johnson	01718
1	MS0352	W. Kent Schubert	01718
1	MS0721	Marjorie L. Tatro	06100
1	MS0734	Ward I. Bower	06111
1	MS1033	Stanley Atcitty	06113
1	MS1033	Abraham Ellis	06112
1	MS1033	Jennifer E. Granata	06112
1	MS1033	Charles J. Hanley	06112
1	MS1033	Scott S. Kuszmaul	06112
1	MS1078	Wahid L. Hermina	01710
1	MS1079	Gilbert V. Herrera	01700
1	MS1082	Anthony L. Lentine	01727
1	MS1082	Jason E. Strauch	01718
1	MS1104	Rush D. Robinett III	06110
1	MS1108	Ross Guttromson	06113
1	MS1108	Benjamin L. Schenkman	06113
1	MS1108	Juan J. Torres	06111
1	MS1318	Bruce A. Hendrickson	01440
1	MS1318	Robert J. Hoekstra	01426
1	MS1321	David A. Schoenwald	01444
1	MS1321	Randall M. Summers	01444
1	MS1322	Sudip S. Dosanjh	01420
1	MS0359	D. Chavez, LDRD Office	01911
1	MS0899	Technical Library	09536 (electronic copy)

Sandia National Laboratories